Title

Cancer epithelia-derived mitochondrial DNA is a targetable initiator of a paracrine signaling loop that confers taxane resistance.

Journal

Proceedings of the National Academy of Sciences of the United States of America, 117(15)

ISSN

0027-8424

Authors

Haldar, Subhash
Mishra, Rajeev
Billet, Sandrine
et al.

Publication Date

2020-04-01

DOI

10.1073/pnas.1910952117

Peer reviewed

Cancer epithelia-derived mitochondrial DNA is a targetable initiator of a paracrine signaling loop that confers taxane resistance

Subhash Haldar[a], Rajeev Mishra[a], Sandrine Billet[a], Manish Thiruvalluvan[a], Veronica R. Placencio-Hickok[a], Anisha Madhav[a], Frank Duong[a], Bryan Angara[a,b], Priyanka Agarwal[a], Mourad Tighiouart[a], Edwin M. Posadas[a], and Neil A. Bhowmick[a,b,1]

[a]Department of Medicine, Samuel Ochin Comprehensive Cancer Institute, Cedars-Sinai Medical Center, Los Angeles, CA 90048; and [b]Department of Research, VA Greater Los Angeles Healthcare System, Los Angeles, CA 90073

Edited by David A. Tuveson, Cold Spring Harbor Laboratory, Cold Spring Harbor, NY, and accepted by Editorial Board Member Rakesh K. Jain March 3, 2020 (received for review June 25, 2019)

Stromal-epithelial interactions dictate cancer progression and therapeutic response. Prostate cancer (PCa) cells were identified to secrete greater concentration of mitochondrial DNA (mtDNA) compared to noncancer epithelia. Based on the recognized coevolution of cancer-associated fibroblasts (CAF) with tumor progression, we tested the role of cancer-derived mtDNA in a mechanism of paracrine signaling. We found that prostatic CAF expressed DEC205, which was not expressed by normal tissue-associated fibroblasts. DEC205 is a transmembrane protein that bound mtDNA and contributed to pattern recognition by Toll-like receptor 9 (TLR9). Complement C3 was the dominant gene targeted by TLR9-induced NF-κB signaling in CAF. The subsequent maturation complement C3 maturation to anaphylatoxin C3a was dependent on PCa epithelial inhibition of catalase in CAF. In a syngeneic tissue recombination model of PCa and associated fibroblast, the antagonism of the C3a receptor and the fibroblastic knockout of TLR9 similarly resulted in immune suppression with a significant reduction in tumor progression, compared to saline-treated tumors associated with wild-type prostatic fibroblasts. Interestingly, docetaxel, a common therapy for advanced PCa, further promoted mtDNA secretion in cultured epithelia, mice, and PCa patients. The antiapoptotic signaling downstream of anaphylatoxin C3a signaling in tumor cells contributed to docetaxel resistance. The inhibition of C3a receptor sensitized PCa epithelia to docetaxel in a synergistic manner. Tumor models of human PCa epithelia with CAF expanded similarly in mice in the presence or absence of docetaxel. The combination therapy of docetaxel and C3 receptor antagonist disrupted the mtDNA/C3a paracrine loop and restored docetaxel sensitivity.

prostate cancer | docetaxel | mtDNA | carcinoma-associated fibroblast

Prostate cancer (PCa) is the second leading cause of cancer-related death of men in the United States (1). Stromal-epithelial interactions define tumor initiation, progression, and therapeutic resistance (2–6). In the prostate tumor microenvironment, stromal fibroblasts coevolve with the cancer epithelia in a reciprocal relationship (7). The central role of cancer-associated fibroblasts (CAF) was recognized when their absence was found to result in reduced tumor volumes (8). Conversely, the combining of nontumorigenic prostatic epithelia with CAF was found to promote tumorigenesis (9, 10). CAF produce paracrine growth factors, proteolytic enzymes, and components of the extracellular matrix, apparently in response to cues from tumor cells (11–14). Prostatic fibroblasts contribute to the androgen signaling axis in prostate development, and CAF are attributed to the development of castrate resistance (2, 3, 15, 16). Paracrine protumorigenic signaling between CAF and the cancer epithelia in contrast to normal tissue-associated fibroblasts (NAF) seems to be a durable result of epigenetic programming in some cases that are able to promote tumor growth (7, 17, 18). However, the mechanisms regulating this cross talk are not well elucidated in the context of chemotherapy. The goal of this study was to better understand how docetaxel treatment, a mainstay for PCa patients with advanced disease, impacts CAF and its role in supporting tumor expansion.

Taxanes, inclusive of docetaxel, paclitaxel, and cabazataxel, hyperstabilize microtubules to inhibit intracellular trafficking and signaling, cause mitotic arrest, and induce apoptotic cell death for numerous solid tumor types, inclusive of ovarian, breast, lung, head and neck, and prostate (19). Docetaxel was the first taxane to provide an overall survival benefit for men with metastatic, castrate-resistant prostate cancer (20). Phase 2 studies have tested the use of taxanes, prior to androgen-targeted therapy failure, and demonstrated positive biochemical tumor response (21, 22). Significantly, the combined use of hormone therapy and docetaxel for castrate-sensitive PCa patients with high-volume localized and metastatic disease provided a significant survival advantage compared to castration therapy alone in two independent randomized trials (23, 24). Despite the importance of taxanes in the management

Significance

The work provides a conceptual advance in functionally defining the cross talk of tumor epithelia with cancer-associated fibroblastic cells contributing to tumor progression and therapeutic resistance. Independent of protein-based signaling molecules, prostate cancer cells secreted mitochondrial DNA to induce associated fibroblasts to generate anaphylatoxin C3a to support tumor progression in a positive feedback loop. Interestingly, the standard of care chemotherapy, docetaxel, used to treat castrate-resistant prostate cancer was found to further potentiate this paracrine-signaling axis to mediate therapeutic resistance. Blocking anaphylatoxin C3a signaling cooperatively sensitized prostate cancer tumors to docetaxel. We reveal that docetaxel resistance is not a cancer cell-autonomous phenomena and that targeting an immune modulator derived from cancer-associated fibroblasts can limit the expansion of docetaxel-resistant tumors.

Author contributions: S.H., R.M., S.B., M. Thiruvalluvan, E.M.P., and N.A.B. designed research; S.H., R.M., S.B., M. Thiruvalluvan, V.R.P.-H., A.M., F.D., B.A., P.A., and N.A.B. performed research; S.H., S.B., M. Thiruvalluvan, M. Tighiouart, and N.A.B. analyzed data; and S.B. and N.A.B. wrote the paper.

Competing interest statement: Part of the work has been submitted for patent protection (S.H. and N.A.B.).

This article is a PNAS Direct Submission. D.A.T. is a guest editor invited by the Editorial Board.

[1]To whom correspondence may be addressed. Email: bhowmickn@cshs.org.

This article contains supporting information online at https://www.pnas.org/lookup/suppl/doi:10.1073/pnas.1910952117/-/DCSupplemental.

First published April 1, 2020.

of PCa, its utility is limited by toxicity and acquisition of chemoresistance. Here, we examine the role of the PCa microenvironment in docetaxel chemoresistance.

There is a large body of evidence describing the role of mitochondrial DNA (mtDNA) in PCa (25–27). Proteins in mitochondrial complexes I, III, IV, and V involved in oxidative phosphorylation are encoded by mtDNA. Mutations found in mtDNA increase tumorigenicity in PCa and deregulated mitochondrial metabolism is known to promote prostate carcinogenesis (26, 28). PCa cells have greater mitochondrial content than benign prostate epithelium, and alterations in mtDNA copy number may reflect disruption of the normal prostate glandular architecture (29, 30). Furthermore, mtDNA instability is a hallmark of human cancers (31). PCa patients are found to have measurable concentrations of mtDNA in serum (32). In this study, we tested the hypothesis that secreted mtDNA functions as a mediator of epithelia-CAF cross talk. We reasoned that the mtDNA could potentially signal adjacent cells through pattern recognition receptors, such as toll-like receptor 9 (TLR9). Many similar pattern recognition receptors are recognized on the surface of immune cells for the defense from bacterial and viral infection. TLR4 is reported to be expressed in skin and lung fibroblasts (33, 34). Recently, we reported the expression of TLR2 and TLR4 activity in gingival fibroblastic cells (35). However, endosomal TLR9 is described in macrophage and dendritic cells signal in response to unmethylated bacterial DNA for the initiation of an inflammasome signaling cascade associated with IL-1β and IL-6 expression (36). We identified a reciprocal signaling cascade initiated by PCa epithelia-derived mtDNA signaling to CAF via TLR9 activity in potentiating a downstream paracrine response on PCa epithelia.

Results

Activation of TLR9 and Anaphylatoxin C3a in Cancer-Associated Fibroblast through Mitochondrial DNA. Based on reported elevation of mtDNA in PCa patient blood (32), we measured the mtDNA content in the conditioned media of prostate cell lines. We found that PCa lines (PC3, LNCaP, and TRAMPC2) expressed 3 to 10 times more mtDNA in the conditioned media than a benign prostate epithelial cell line, BPH1 (Fig. 1*A*). To determine if there was a paracrine impact of mtDNA signaling in CAF, we incubated CAF cells with conditioned media from LNCaP (LNCaP-CM) for the expression of the mtDNA cognate receptor TLR9 and its downstream effectors. TLR9 messenger RNA (mRNA) expression was found to be significantly up-regulated by LNCaP-CM in CAF, compared to NAF or treatment of either CAF/NAF with BPH1-CM (*SI Appendix*, Fig. S1*A*). Examining the DNA content of the LNCaP-CM, we found that the amount of mtDNA was ∼10-fold greater than telomeric DNA (*SI Appendix*, Fig. S1*B*). PCa epithelial conditioned media treatment of CAF resulted in up-regulation of TLR9 and downstream phosphorylated TAK1, NF-κB p65 phosphorylation, cleaved-caspase1, and IL-1β protein expression (Fig. 1*B* and *SI Appendix*, Fig. S1*C*). As exosome-mediated transfer of mtDNA was a possibility, we treated CAF cells with ultracentrifuge-enriched exosomes generated by LNCaP cells as well as exosome-depleted LNCaP-CM. We found that the exosome-depleted LNCaP-CM induced TAK1, NF-κB signaling, and C3a expression in CAF, comparable to unaltered LNCaP-CM (*SI Appendix*, Fig. S1*D*). However, the exosome-enriched fresh media did not seem to induce the same signaling axis. This finding was corroborated by inhibiting exosome generation, as the LNCaP cells with the dynamin inhibitor, dynasore (37), showed no appreciable changes in mtDNA content in the media (*SI Appendix*,

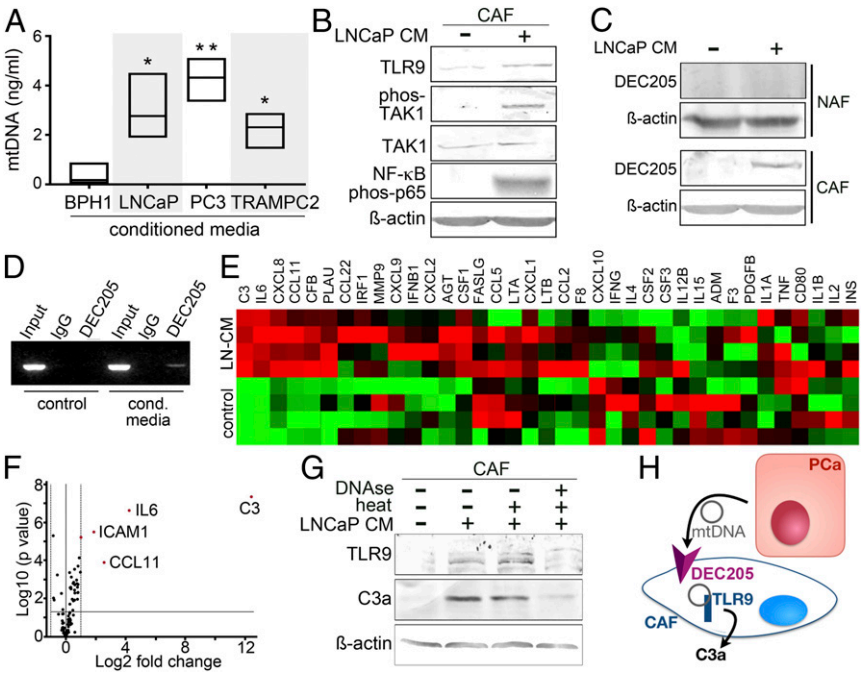

Fig. 1. Activation of TLR9 and C3a by mtDNA. (*A*) mtDNA was measured from conditioned medium (CM) of prostatic epithelia after 48 h of incubation (n = 3). (*B*) Protein expression in CAF treated with LNCaP-CM was visualized by Western blot. (*C*) DEC205 expression was measured in NAF and CAF treated with LNCaP-CM by Western blot. (*D*) DEC205 was immunoprecipitated, cross-linked, and subjected to mtDNA PCR amplification for MT-CO_2 following CAF incubation with fresh RPMI or LNCaP-CM. CAF cell lysate prior to immunoprecipitation or IgG immunoprecipitant was used as total input and negative controls, respectively. (*E*) mRNA expression profiles of the NF-κB–signaling targets in CAF incubated with LNCaP-CM were compared to control-CM in the heat map (n = 4). (*F*) Volcano plot showing distribution of differential mRNA expression levels in CAF and CAF incubated with LNCaP-CM. While only secreted proteins were illustrated in the heat map, all 84 NF-κB target genes were represented in the volcano plot. (*G*) TLR9 and anaphylatoxin C3a protein expression was visualized in CAF incubated with LNCaP-CM incubated with or without DNase1 treatment. DNase activity was heat inactivated after 10 min. (*H*) MtDNA secreted by PCa epithelia signal CAF by binding DEC205 and subsequent TLR9-mediated anaphylatoxin C3a expression. *P < 0.05, **P < 0.01.

Fig. S1*E*). Since TLR9 is a cytoplasmic receptor, we sought to identify a mediator for DNA entry into the cell. Candidate mediators with the capacity to bind DNA, such as HMGB1, HMGA2, and DEC205, were found to be expressed by CAF in response to LNCaP-CM (*SI Appendix*, Fig. S1*F*). HMGB1 expression, previously associated Toll like receptor signaling, was similarly induced by both NAF and CAF cells in response to LNCaP-CM. HMGA2 expression, demonstrated to promote cell proliferation, was constitutively expressed regardless of LNCaP-CM treatment. However, LNCaP-CM induced DEC205 protein expression in CAF, but not NAF (Fig. 1*C*). DEC205 (LY75) is a transmembrane endocytic receptor reported to bind and internalize unmethylated CpG by dendritic cells (38). Due to its differential expression in CAF and NAF cells, the binding capacity of DEC205 to mtDNA was tested in CAF through an adaptation of chromatin immunoprecipitation, termed mtDNA immune precipitation (mDIP). The mitochondrial MT-CO_2 gene was PCR amplified following immunoprecipitation of DEC205 in the presence of LNCaP-CM, but not in its absence (Fig. 1*D*). Following discovery that NF-κB signaling in CAF was a result of PCa-derived mtDNA, we performed a focused qPCR array to determine the effect of NF-κB on downstream target genes. As expected, LNCaP-CM induced the expression of multiple inflammatory cytokines by CAF, including IL-6, CXCL8, and CCL11 (Fig. 1*E*). Interestingly, complement C3 was upregulated by >12 Log_2-fold with LNCaP-CM over control, the greatest differentially expressed gene in CAF cells (Fig. 1*F*). The role of complement C3 action is central to the innate immune response to bacterial and viral infection. C3 has also been implicated in potentiating tumor cell growth (39). However, the active component, anaphylatoxin C3a, is a product of a tightly regulated proteolytic cleavage of C3 (40). Interestingly, we found that LNCaP-CM–induced TLR9 and C3a expression by CAF was sensitive to DNase treatment (Fig. 1*G*). Thus, mtDNA secreted by PCa epithelia can bind DEC205 on the cell surface of CAF and activate TLR9 and C3a maturation (Fig. 1*H*).

To explore the role of TLR9 in C3a expression, prostatic fibroblasts from wild-type and TLR9-knockout mice were treated with CpG oligonucleotides, ODN 1826 (synthetic ligand for TLR9, CpG-ODN), or LNCaP-CM. TLR9 and phosphorylated TAK1 was up-regulated by CpG-ODN (Fig. 2*A*). Further up-regulation of TLR9 and TAK1 was observed with incubation with LNCaP-CM. DNase1 treatment of LNCaP-CM reduced TLR9 protein expression as well as C3a expression by wild-type mouse fibroblasts. TAK1 phosphorylation and anaphylatoxin C3a expression by LNCaP-CM was found to be dependent on TLR9 expression. However, treating the wild-type prostatic fibroblasts with CpG-ODN generated dramatically less anaphylatoxin C3a compared to treatment with LNCaP-CM, similar to that found when LNCaP-CM was treated with DNase1. Enzyme-linked immunosorbent assay (ELISA)-based quantitation of C3a secretion by CAF corroborated expression when incubated with TRAMPC2-CM or LNCaP-CM, but negligible expression when incubated with CpG-ODN (Fig. 2*B*). These results show that PCa epithelial secretion of mtDNA could promote TLR9 signaling and anaphylatoxin C3a expression by CAF, whereas CpG alone could activate TLR9 but was not sufficient for C3 protein maturation.

Complement processing can occur through an enzymatic activation cascade or alternative pathways culminating in the cleavage of complement C3 (41). Cleavage products of C3 are well described for microbe opsonization and activation of proinflammatory signaling. As the classical pathway involves the complex of complement proteins C1b and C2b for C3 cleavage, this was not a likely mechanism in cultured fibroblasts. Therefore, the alternative pathway involving reactive oxygen-mediated cleavage was tested (42). Not surprisingly, the treatment of CAF with LNCaP-CM resulted in reactive oxygen generation, as revealed by 2′,7′-dichlorofluorescin diacetate (DCFDA) fluorescent signal using fluorescence-activated cell sorting (FACS) analysis and visualized by fluorescent microscopy (Fig. 2 *C* and *D*). CpG-ODN treatment promoted no such reactive oxygen signal and *N*-acetylcysteine

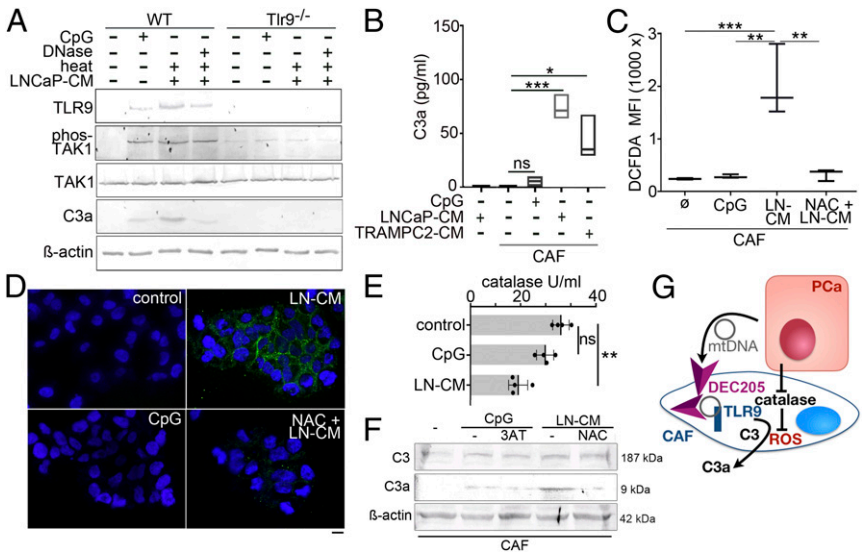

Fig. 2. Mechanism of C3a generation by CAF. (*A*) TLR9 signaling was tested in mouse prostatic fibroblasts from cultured wild type (WT) or TLR9-knockout (TLR9$^{-/-}$) mice treated with CpG-ODN or LNCaP-CM in the presence and absence of DNase1 treatment. (*B*) Secreted C3a was measured by ELISA from CAF and NAF conditioned media following treatment with CpG-ODN, LNCaP-CM, or TRAMPC2-CM ($n = 3$). (*C*) Flow cytometry was used to quantitate intracellular reactive oxygen by DCFDA fluorescence in CAF incubated with control, CpG-ODN, or LNCaP-CM DCFDA^{+} cells, absent the dead cell marker (7-amino-actinomycin D), were quantitated. (*D*) Cytoplasmic green DCFDA was localized with DAPI nuclear counter stain by fluorescence microscopy. (Scale bar, 16 μm.) (*E*) Catalase activity was quantitated in CAF following incubation with fresh media (control), CpG-ODN, or LNCaP-CM. (*F*) Protein expression of complement C3 and anaphylatoxin C3a in CAF was Western blotted. The CAF were incubated with either CpG-ODN in the presence and absence of the catalase inhibitor 3-amino-1,2,4-triazole (3AT) or LNCaP-CM in the presence or absence of reactive oxygen inhibitor *N*-acetyl cysteine (NAC). (*G*) mtDNA from in LNCaP-CM binds DEC205 for internalization in CAF cells for subsequent TLR9 signaling. LNCaP-CM inhibition of catalase activity allows ROS accumulation to facilitate C3a maturation in the CAF. *$P < 0.05$, **$P < 0.01$, ***$P < 0.001$, and ns, not significant.

(used as a reactive oxygen inhibitor) suppressed LNCaP-CM–induced reactive oxygen as well as anaphylatoxin C3a maturation. As catalase can mitigate the reactive oxygen content of cells, its activity was measured in CAF. We found that catalase activity in CAF was significantly suppressed by LNCaP-CM, compared to either untreated control or CpG-ODN treatment (Fig. 2*E*). Western blotting demonstrated that *N*-acetylcysteine supplementation blocked the conversion of C3 to C3a induced by LNCaP-CM (Fig. 2*F*). However, the inhibition of catalase by 3-amino-1,2,4-triazole did not improve anaphylatoxin C3a generation when combined with CpG-ODN. Ultimately, both CpG-ODN and LNCaP-CM induced C3 expression in CAF, but anaphylatoxin C3a generation was dependent on the suppression of catalase activity as well as on the induction of reactive oxygen by LNCaP-CM (Fig. 2*G*).

C3a Signaling Enhances PCa Expansion. In an effort to determine a reciprocal epithelial response to anaphylatoxin C3a expressed by CAF, we tested the impact of established complement agonists and antagonists on PCa expansion. We found that LNCaP, PC3, and TRAMPC2 all expressed the anaphylatoxin C3a receptor (C3aR, *SI Appendix*, Fig. S2*A*). Although HMGB1 was heterogeneously expressed by the three epithelial cell lines, negligible expression of DEC205, TLR9, or C3a reinforced the requirement of a paracrine TLR9-mediated anaphylatoxin C3a-signaling axis (*SI Appendix*, Fig. S2*B*). Coculturing of CAF and TRAMPC2 cells in transwells demonstrated that the knockdown of C3aR in TRAMPC2 by small interfering RNA (siRNA) resulted in reduced Ki67^{+} epithelial proliferative cells, compared to scrambled control siRNA (*SI Appendix*, Fig. S2*C*). Next, the effect of C3a signaling on PCa cells was tested by incubating LNCaP, PC3, and TRAMPC2 with an C3aR agonist or scrambled peptide. Agonist peptides to C3aR were used rather than C3a itself because anaphylatoxins are extremely labile (43). Exposure of 0.1 μM C3aR agonist for 48 h increased proliferation, as measured by Ki67 expression, in LNCaP (28%), PC3 (30%), and TRAMPC2 (21%) compared to scrambled peptide-treated cells (*SI Appendix*, Fig. S2*D*). The C3aR agonist was further found to promote phosphorylation of AKT and downstream MAP kinase signaling by phosphorylation of p42/44 MAPK (p-ERK1/2, Fig. 3*A*). The up-regulation of BCL2 was identified as a downstream signaling target of AKT in support of cell survival.

To validate the observation of C3a signaling, we allografted mouse prostatic fibroblasts with PCa epithelia into syngeneic C57B/6 mice. We grafted either wild-type or TLR9-knockout fibroblasts and recombined them with luciferase-expressing TRAMPC2 cells under the renal capsule. After the tumors were visible by bioluminescent imaging, the mice hosting wild-type prostatic fibroblast grafts were treated with either vehicle (control) or SB290157, a C3aR antagonist. Within 3 wk of grafting, the vehicle-treated tumors with wild-type fibroblasts expanded reproducibly; however,

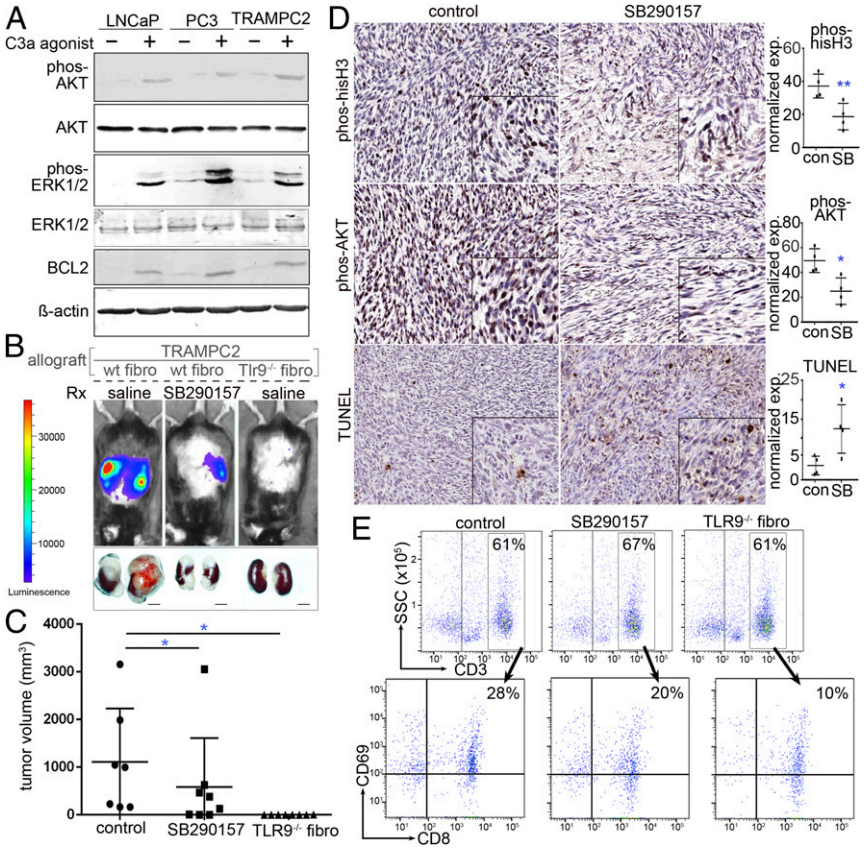

Fig. 3. Role of C3a in PCa progression. (*A*) PCa cell lines incubated in the absence and presence of C3a receptor agonist peptide (48 h) was Western blotted for cell survival and proliferation protein expression. (*B*) C57BL/6 mice were allografted with tissue recombinants of luciferase-expressing TRAMPC2 with wild-type (wt) or Tlr9$^{-/-}$ fibroblasts. The mice were treated with saline or the TLR9 antagonist SB290157. Luciferase bioluminescence was used to image tumor progression. (*C*) Mean tumor volume (mm^3) and SD for each treatment condition are depicted (*$P < 0.05$, $n = 8$). (*D*) Immunohistochemistry for phosphorylated AKT, phosphorylated histone-H3, and TUNEL staining of the tumor tissues were performed and quantitated. Hematoxylin was used as a nuclear counterstain. The corresponding graphs illustrate the mean and SD expression of the staining ($n = 4$). Statistical significance was determined by one-way ANOVA (*$P < 0.05$, **$P < 0.01$). (*E*) FACS analysis of the tumor-draining lymph nodes demonstrated that control, C3a antagonist, and TLR9-knockout fibroblasts had similar CD3^{+} T cell infiltration; however, their activation state as determined by CD8^{+}/CD69^{+} expression differed significantly.

SB290157 had significantly reduced tumor size (Fig. 3 *B* and *C*). Interestingly, the allografts with TLR9-knockout fibroblasts had negligible tumor growth, confirming that the role of the associated paracrine-signaling axis is dependent on TLR9 and C3a. We were able to perform immunohistochemistry only on the grafts with wild-type fibroblasts and TRAMPC2 as not enough tissue was available from grafts with TLR9-knockout fibroblasts. Tumor cell mitosis, as determined by phosphorylated histone H3 expression, was significantly lower when the host mice were treated with SB290157 (Fig. 3*D*). The activation of AKT, localized by phosphorylated AKT staining, was elevated in the tumor cells allografted with wild-type fibroblasts and reversed by SB290157 treatment. The C3aR antagonist was found to significantly elevate tumor cell death, as localized by terminal deoxynucleotidyl transferase dUTP nick end labeling (TUNEL) staining.

Complement anaphylatoxins have a wide spectrum of proinflammatory effects. Anaphylatoxin C3a is particularly regarded for the chemotaxis of myeloid cells and T cells (44–47). We could not consistently profile the immune infiltrates within the tumor as tissue was limited in some treatment conditions; therefore, the draining lymph nodes were evaluated. We observed a similar reduction of myeloid-derived suppressor cells ($CD11b^+$, $Ly6G^+$) with SB290157 and $TLR9^{-/-}$ fibroblasts, compared to control saline-treated mice with TRAMPC2/wild-type fibroblasts (*SI Appendix*, Fig. S3). An approximately threefold reduction of M2 macrophage activation ($F4/80^+$, $CD208^+$, $CD69^+$) was observed in SB290157-treated mice and $TLR9^{-/-}$ fibroblast-associated tumors, compared to control by FACS analysis. As T lymphocytes are confirmed regulators of tumor progression and known to respond to anaphylatoxin C3a (48), we measured the impact of C3a antagonism on T cell recruitment to the tumors. Interestingly, $CD3^+$ T cells on the whole showed similar recruitment to the tumor-draining lymph nodes regardless of C3a antagonist or fibroblast TLR9 status (Fig. 3*E*). However, $CD8^+$ T cell activation, as determined by the expression of the costimulatory molecule $CD69^+$, was appreciably down-regulated by C3a antagonist and further down-regulated in tumors with TLR9-knockout fibroblasts. Under the same conditions, there was little change in T_{reg} ($CD3^+$, $CD4^+$, $CD25^+$, $FoxP3^+$) recruitment, but Th17 cell ($CD3^+$, $CD4^+$, $CD25^+$, $ROR\gamma^+$) recruitment was elevated by SB290157 treatment and $TLR9^{-/-}$ fibroblasts (*SI Appendix*, Fig. S4). However, only half the activated T helper cells ($CD3^+$, $CD4^+$, $CD25^+$, $CD69^+$) were recruited to the $TLR9^{-/-}$ fibroblast-associated tumors, compared to either control or SB290157 treatment. Since functions of T helper cells include the activation of cytotoxic T cell and macrophage, the diminished recruitment of T helper cells in the $TLR9^{-/-}$ fibroblast-associated tumors could support the reduced activation of cytotoxic T cells and M2 macrophage activation in these tumors. The further increase in Th17 (T helper-17) cell recruitment in the SB290157-treated and $TLR9^{-/-}$ fibroblast-associated tumors support the general immune-suppressive state of these tumors. Thus, the resulting changes in tumor size were minimally affected by immune surveillance and likely driven by the reciprocal tumor epithelial-fibroblast interaction.

Synergistic Effect of Docetaxel and C3aR Antagonism Inhibit Tumor Expansion. Based on the observed activation of AKT by anaphylatoxin C3a in PCa epithelia, we were curious as to the role of this prosurvival signal in the context of a mediator of cell death such as chemotherapy. To determine the clinical relevance of the TLR9/C3a-signaling axis in PCa patients, we measured plasma mtDNA content in men within 2 wk prior to treatment and while undergoing docetaxel treatment (within 4 to 8 wk of start) in a paired fashion. Docetaxel induced a dramatic increase in circulating mtDNA in the PCa patients ($P = 0.006$, Fig. 4*A*). In parallel, mice treated with docetaxel (6 mg/kg/wk) for 3 wk showed significant elevation of plasma mtDNA content ($P < 0.05$, Fig. 4*B*). In examining the direct effect of docetaxel on PCa epithelia, we found docetaxel to profoundly elevate mtDNA secretion by LNCaP, PC3, and TRAMPC2 cells in a dose-dependent manner (Fig. 4*C*). As a control, nontumorigenic BPH1 cells were also found to secrete more mtDNA in response to docetaxel, but at levels approximately a tenth of that observed in LNCaP cells (*SI Appendix*, Fig. S5*A*). Incidentally, higher doses of docetaxel were used for PC3 cells compared to the other two lines due to its inherent resistance. The influence of stromal-epithelial cross talk in the development of docetaxel resistance was tested in co-culture studies within a three-dimensional (3D) matrix of collagen I and Matrigel (4, 18). The coculture of PC3 and CAF resulted in a doubling of $EpCAM^+/Ki67^+$ proliferative epithelia compared to that when PC3 cells were grown alone (Fig. 4*D*). Additional treatment with docetaxel did not appreciably reduce the CAF-induced proliferative epithelial fraction. The C3aR antagonist restored the sensitivity of PC3 cells to docetaxel in coculture. Drug interaction studies reveled that low doses of SB290157, with little-to-no intrinsic impact on PC3 survival alone, sensitized the otherwise resistant PC3 cells to docetaxel in

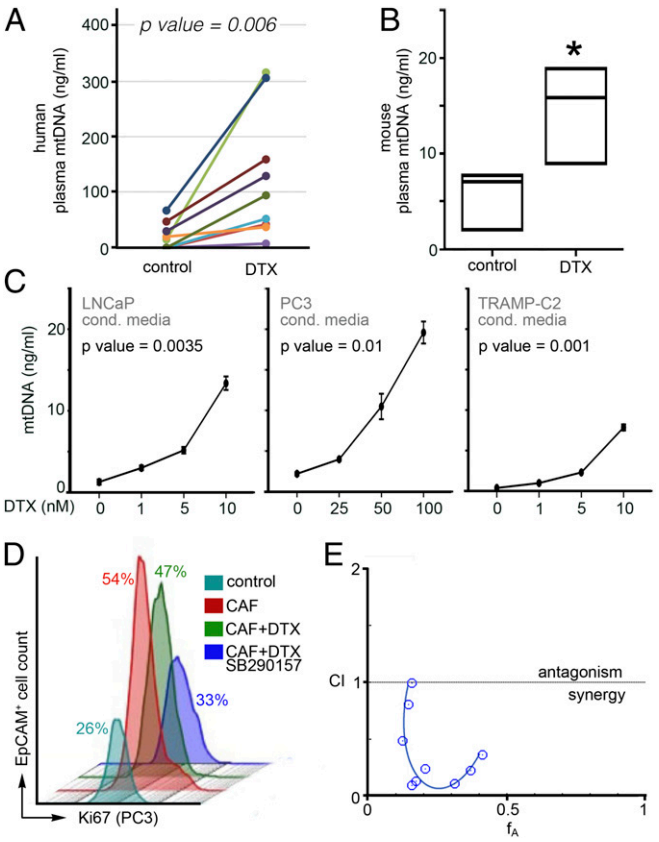

Fig. 4. Docetaxel promotes mtDNA release from PCa cells, and paracrine TLR9 signaling contributes to therapeutic resistance. (*A*) Plasma levels of mtDNA were quantified from PCa patients before and after docetaxel treatment ($n = 9$). (*B*) mtDNA content of plasma from mice treated with docetaxel was quantitated ($n = 3$). Data represent the mean ± SD; $^*P < 0.05$. (*C*) mtDNA secreted by PCa cell lines treated with docetaxel was elevated in a dose-dependent manner ($n = 3$). Significance was determined by repeated measures ANOVA. (*D*) Treatment of a 3D coculture model of PC3 and CAF cells with docetaxel and the TLR9 antagonist SB290157 supported differential epithelial proliferation as determined by quantitating $EPCaM^+/K_i\text{-}67^+$ cells by FACS analysis ($n = 3$). (*E*) Synergistic cooperativity was identified in PC3 cell viability measured by MTT assay following treatment with docetaxel and SB290157 through the Chou-Talalay method ($n = 4$). Values below the confidence interval (CI) of 1 are considered a synergistic combination.

a synergistic manner (fractional inhibitory concentration index <0.5; Fig. 4*E* and *SI Appendix*, Fig. S5*B*).

The therapeutic significance of the observed stromal-epithelial cross talk was tested in male nude mice with tissue recombinant xenografts of CAF and PC3 cells. Tumor growth curves indicated that tumor volume was not significantly reduced by treatment with the low dose of docetaxel (6 mg/kg/wk) alone, compared to vehicle treatment (Fig. 5*A*). However, the combined treatment of docetaxel and SB290157 significantly limited tumor growth ($P < 0.05$). No significant impact on the body weight was observed in any treatment groups, which supports a low-dose taxane therapy strategy with reduced toxicity (*SI Appendix*, Fig. S5*C*). Western blotting of the tumor tissues revealed the activation of TAK1, AKT, and ERK1/2 in docetaxel-treated mice compared to vehicle treatment (Fig. 5*B*). The up-regulation of plasma mtDNA in docetaxel-treated mice supported the elevated phosphorylation of TAK. SB290157 treatment reduced AKT and ERK1/2 phosphorylation induced by docetaxel. Importantly, BLC2 was reduced by the combination therapy. Histology of the tumors and immunohistochemistry of the corresponding tissues allowed us to localize and quantitate the relevant signaling molecules (Fig. 5*C* and *SI Appendix*, Fig. S5*D*). The significant docetaxel induction of phosphorylated TAK1, C3, and TUNEL staining was not significantly altered by C3 antagonism. However, docetaxel-treatment–induced AKT phosphorylation was diminished by SB290157 treatment. In parallel, docetaxel reduced mitosis, indicated by phosphorylated histone-H3 localization, that was further down-regulated by SB290157 treatment. Combining low doses of docetaxel with C3aR antagonism ultimately limited tumor growth.

Discussion

Our data show that reciprocal paracrine signaling between PCa and associated fibroblasts promotes cancer progression and facilitates docetaxel resistance. We hypothesized that mtDNA could be the paracrine-signaling molecule generated by PCa cells (Fig. 6). The docetaxel-induced mtDNA secretion from PCa cells into the tumor microenvironment was significantly greater than

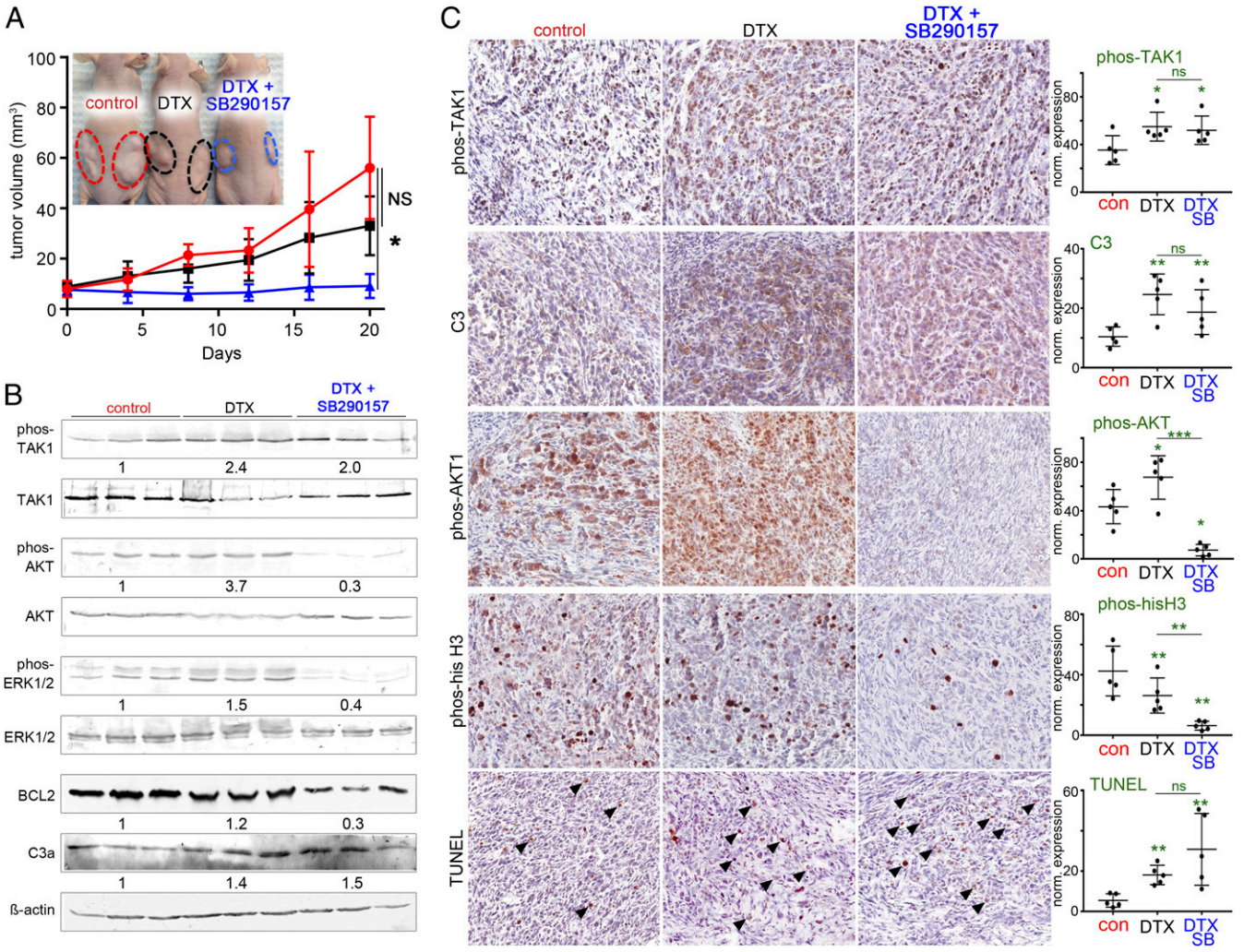

Fig. 5. Synergistic effect of docetaxel and SB 290157 inhibits tumor growth. (*A*) Subcutaneous xenografts of PC3 and CAF tumor volumes were longitudinally measured. When tumor average volume reached 80 mm^3, mice were treated with vehicle or docetaxel in the presence or absence of SB290157 for 20 d ($n = 4$). Representative images show each group of mice (*Inset*). (*B*) Western blots of the tumor tissues for the respective treatments are shown with the mean quantitation for each condition displayed below ($n = 3$). (*C*) Immunolocalization of phosphorylated TAK1, complement C3, phosphorylated AKT, phosphorylated histone H3, and TUNEL expression in tumor tissues (brown) was counterstained with hematoxylin (blue). The corresponding graphs illustrate the mean and SD expression of the respective staining ($n = 5$). Arrowheads indicate positive staining. Statistical significance was determined by one-way ANOVA (*$P < 0.05$, **$P < 0.01$). ns, no statistical significance.

the basal levels of mtDNA secreted by PCa cells. Accordingly, prostate tumors in both murine models and men harboring prostate tumors demonstrated elevated circulating mtDNA when treated with docetaxel. For subsequent CAF signaling, the mtDNA required entry into the cytoplasm for TLR9 activation. Based on the previous demonstration of DEC205 capture of CpG in dendritic cells (38), a similar scenario was explored for the prostatic CAF. Instead of unmethylated bacterial DNA, we demonstrated that, in fact, DEC105 could directly bind mtDNA on CAF cells for classic pattern recognition receptor TLR9 activation of TAK1 and NF-κB (49). TLR9 was identified to be essential for complement C3 expression by CAF in response to mtDNA, but the accumulation of reactive oxygen driving C3 cleavage and anaphylatoxin C3a generation was dependent on PCa epithelial interaction. Released anaphylatoxin C3a in the tumor microenvironment increased proliferation of cancer cells and potentiated resistance to docetaxel treatment.

It is apparent that PCa-induced paracrine NF-κB activation in CAF dramatically potentiated complement C3 expression over other known NF-κB targets (Fig. 1). There is a well-described immune defense for bacterial pathogens that includes Toll-like receptor-mediated complement expression and generation of anaphylatoxins (50). However, the novel mechanism of TLR9 induction by PCa-derived mtDNA paracrine signal transduction mechanism in CAF cells was not observed by NAF cells (Fig. 1). Cell-free circulating mtDNA release in plasma at low levels under cellular stress is reported in instances of cancer, trauma, infections, stroke, and autoimmune, metabolic, and rheumatic diseases (51, 52). While activated T cells can signal dendritic cells through exosome-based delivery of mtDNA (53), this was not necessarily the means of paracrine communication between PCa and CAF. Exosome depletion of LNCaP-CM and dynamin inhibition LNCaP cells had little effect on TAK1 and C3a expression by CAF (*SI Appendix*, Fig. S1). Uniquely, DEC205 was expressed by CAF in the context of PCa epithelial-conditioned media for endocytic delivery of mtDNA and TLR9 activation. Docetaxel further potentiated PCa release of mtDNA by over threefold in multiple cell lines (Figs. 1 and 4). The expression of TLR9 and C3a was similarly induced by LNCaP-CM by human CAF and wild-type mouse prostatic fibroblasts (Figs. 1 and 2). The activation of the complement system in response to pathogens involves three major pathways: 1) the classical pathway, via antigen-antibody complexes; 2) the lectin pathway, via binding of pattern-recognizing mannose-binding lectins; and 3) the alternative pathway, via any permissive microbe surfaces (41). In all three complement activation pathways, the C3 convertase complex cleaves C3 molecules to form anaphylatoxin C3a. Yet another mechanism of C3 conversion identified in neutrophils involving hydrogen peroxide-related oxygen radicals, such as hypochlorite (42), was the mechanism considered for the stromal-epithelial signaling axis. We found catalase inhibition in CAF to be essential for reactive oxygen species (ROS) accumulation and maturation of anaphylatoxin C3a (Fig. 2). These findings supported the absence of C3 cleavage in CpG-ODN–treated CAF cells despite NF-κB activation.

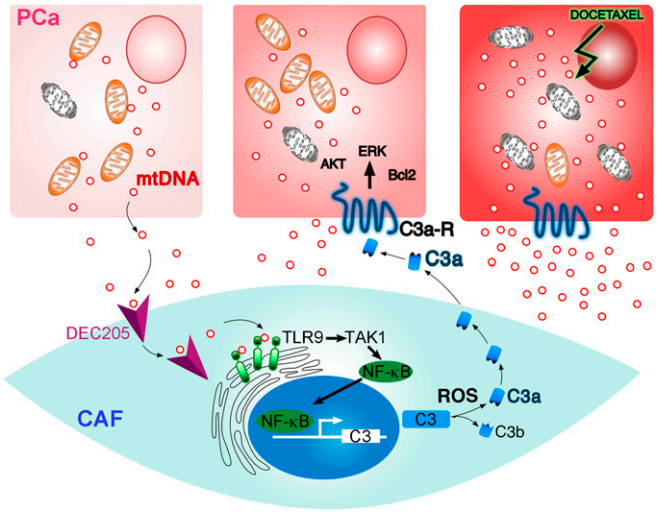

Fig. 6. Illustration of the PCa epithelia and CAF reciprocal interaction. PCa cells generate mtDNA that can bind DEC205 on the cell surface of CAF. TLR9 signaling downstream of epithelial-derived mtDNA results in NF-κB–mediated C3 expression. The accumulation of ROS in CAF facilitated C3a maturation and paracrine signaling with PCa cells to enable cell survival and proliferation. Docetaxel treatment of PCa cells results in expanded secretion of mtDNA in perpetuating C3a expression by CAF further.

Our findings provide a paradigm in which the activation of complement by CAF was distinct from its immunogenic role in promoting tumor growth. Complement proteins can indirectly affect cancer growth by their impact on the host's innate immune response to the tumor. Antagonizing C3aR signaling with SB290157 or the fibroblastic knockout of TLR9 significantly inhibited tumor expansion, all of the while immune cell infiltration was found to have shifted to a general immune-suppressive state (Fig. 3). The reduced recruitment of activated M2 macrophage and activated T helper cell was associated with positive recruitment of Th17 cells when TLR9/C3a signaling was inhibited (*SI Appendix*, Figs. S3 and S4). These findings reveal a rational for the observed reduction in activated cytotoxic T cell recruitment by the C3 antagonist that was further diminished to nearly one-third of the control tumors with TLR9-knockout fibroblasts. In agreement, Wang et al. (54) showed that B16 melanoma growth was slower in C3-deficient mice than in wild-type mice, which suggests a direct role of anaphylatoxin C3a. Tumor AKT, ERK1/2, and BCL2 activation/up-regulation was dependent on fibroblastic TLR9 and epithelial anaphylatoxin receptor signaling. Knocking down C3aR in TRAMPC2 significantly reduced its proliferative capacity when cocultured with fibroblasts (*SI Appendix*, Fig. S2). The immune-independent C3a activity acted directly on the tumor cells in a paracrine manner.

Docetaxel resistance is major clinical problem in many cancers including PCa. Activation of several survival signaling pathways (e.g., AKT and ERK with BCL2 expression) can promote a resistant phenotype in response to docetaxel treatment. The potential for mtDNA secretion resulting from cell death was ruled out by parallel apoptosis measurements made with mtDNA quantitation. Incidentally, when lymphocytes secrete mtDNA in response to viral infection, it is not associated with cell death (55). However, since mitophagy is a documented process associated with taxane therapy, only fragments of the mitochondrial genome would likely be found in the media or circulation (56) with high susceptibility for further degradation. CAF reciprocated the PCa-derived mtDNA signal by the TLR9-C3 paracrine axis to trigger cell proliferation in PCa cells in the context of docetaxel (Fig. 5). Remarkably, the synergism of docetaxel and SB290157 was able to sensitize an otherwise resistant PC3 cell line to reduced docetaxel doses to effectively limit tumor growth. Better understanding of stromal complement signaling by cancer cells is needed, as its implications can have a far-reaching impact on many cancer types currently treated with taxanes. With docetaxel in clinical trials in combination with immune checkpoint inhibition therapy, there is potential for a limited activation of infiltrating cytotoxic T cells due to the mtDNA/anaphylatoxin C3a signaling axis. Thus, one must consider the benefits to immune surveillance induced by docetaxel with the tumor-intrinsic proliferative role of complement signaling.

A final implication of our results is that fibroblast response to taxane therapy is consequential to cancer epithelial therapeutic response. Circulating mtDNA has been reported to be a poor

prognostic indicator for PCa patients (32). However, with the limited number of patients analyzed, we were unable to demonstrate a correlation with the level of mtDNA in circulation with the length of docetaxel responsiveness. While the epithelial response to docetaxel can be uncoupled from that of the stromal fibroblasts, the stromal influence on therapeutic resistance is a result of paracrine signaling initiated by the PCa epithelia. We cannot rule out the direct impact of docetaxel on CAF that could also influence epithelial viability. It should be noted that TLR-mediated NF-κB signaling is not a phenomenon limited to mammals. It was originally identified in *Drosophila* (Toll), with Toll9 involved in hematopoietic and digestive tract development (57). Although NF-κB regulation remains conserved, the gene targets are species, tissue, and cell-type specific; in prostatic CAF, DEC205 expression was a determinant of NF-κB signaling. The fact that NF-κB exquisitely mediates complement C3 expression by CAF and myeloid cells suggests that the hardwiring of this pathway originates in cells of mesenchymal origin. The mechanism revealed here demonstrates that tumors can repurpose the pathogen defense axis for chemotherapy resistance.

Methods

Cell Culture and Animal Experiments. Cultured LNCaP, TRAMPC2, and PC3 (all from ATCC) were grown in Roswell Park Memorial Institute (RPMI) media supplemented with 5% fetal bovine serum and treated with docetaxel (SanofiAventis) or SB290157 (1 μM, Calbiochem) for 48 h. Conditioned medium was treated with DNase1 (0.1 mg/mL, Sigma-Aldrich) in 37 °C for 1 h followed by heat inactivation. Cultured primary NAF and CAF derived in our laboratory (4) were treated with LNCaP-CM, CpG-ODN (5 μM, InvivoGen), and *N*-acetylcysteine (10 mM [Sigma-Aldrich]).

Three-dimensional organotypic coculture was performed in a collagen matrix as previously reported (4). PC3 and CAF were combined in a 1:3 ratio in collagen matrix contain 50% rat tail collagen I, 20% of Matrigel, 10% of 10× Dulbecco's Modified Eagle Media (DMEM) and 1× ready DMEM 5%, 1× ready RPMI 5%, fetal bovine serum 5%, and Nu serum 5%. Cells were treated with docetaxel and SB290157 for 48 h after 72 h of expansion in the matrix. The cells were dissociated from the matrix with collagenase and dispase for Ki67 FACS analysis. FlowJo software (Tree Star Inc.) was used for FACS analysis.

Male C57BL/6 or Nude mice aged 7 to 8 wk were housed in a pathogen-free environment at the Cedars-Sinai Medical Center Animal Facility under the approval of the Institutional Animal Care and Use Committee (# 3679). Subrenal capsule was performed with wild-type mouse fibroblasts (6×10^5) or TLR9$^{-/-}$ mouse fibroblasts (6×10^5) combining with mouse prostate epithelial cell TRAMP-C2 (2×10^5). Treatment with SB290157 (SantaCruz Biotechnology Inc.; 1 mg/kg; [intraperitoneally (i.p.)] daily) was started after 2 wk of grafting in C57BL/6 mice and continued for 5 wk with longitudinal bioluminescent monitoring. Subcutaneous xenografts were done by combining PC3 (5×10^5) and CAF (15×10^5) in Nude mice. Grafts were monitored by caliper throughout the time course of treatment with docetaxel (6 mg/kg/wk) and SB290157 (1 mg/kg; i.p. daily). All indicated tissues were harvested after 5 wk of treatment were fixed in paraffin embedded for immunohistochemistry or immunoblot analysis or dissociated for FACS analysis.

Immunodetection. Paraffin-embedded tissue was processed for immunohistochemical localization was performed with antibodies against p-AKT, p-TAK, p-histoneH3 (Cell Signaling), C3 (Santa Cruz Biotechnology), and TUNEL (Thermo Fisher Scientific) as previously described before (58, 59). All of the slides were scanned using Leica SCN400 (Leica Micro System) and analyzed by Tissue IA Optimizer (Leica). The values of positively stained cells were measured in an unbiased manner. C3a concentration of cultured medium and serum was assayed by sandwich ELISA using a human C3a ELISA kit (BD Bioscience) according to the manufacturer's instructions. Western blots separated by 10, 12, or 15% sodium dodecyl sulfate/polyacrylamide gel electrophoresis were incubated with primary antibodies for TLR9, DEC205 (LS Bio Seattle), phospho-TAK1, TAK1, phospho-AKT, AKT, phospho-ERK1/2, ERK, BCL2 (Cell Signaling), and C3 (Santa Cruz Biotechnology). Western blots were visualized using alkaline phosphatase-conjugated secondary antibodies (Sigma-Aldrich). The ELISA for anaphylatoxin C3a was performed according to manufacturer guidelines (LSBio).

DNA Quantitation. Total DNA from serum or cultured medium was isolated by a Quick-cfDNA Serum and Plasma kit (Zymo Research). The purified DNA were PCR amplified by the mitochondria-specific MT-CO_2 gene (using the following primers: 5′-CCT GCG ACT CCT TGA CGT TG-3′ and 5′-AGC GGT GAA AGT GGT TTG GTT-3′). Quantitation was achieved through the use of a standard curve generated from known purified mtDNA by real time PCR. Telomere-specific sequence $(TTAGGG)_{14}$ was measured using the TRAPEZE RT Telomerase Detection Kit (Millipore).

mDIP. We followed the manufacturer's chromatin immunoprecipitation protocol of Zymo-Spin CHIP Kit (Zymo Research). Briefly, mtDNA from conditioned medium was immunoprecipitated either by normal rabbit IgG antibodies as a negative control or by anti-DEC205 antibody (Santa Cruz Biotechnology). A total of 100 ng of mitochondrial DNA was added to condition medium as a positive control. Nonimmunoprecipitated DNA was used as total input control. The purified immunoprecipitated DNA was PCR amplified by mitochondria-specific primers (MT-CO_2) as mentioned above and was compared to input DNA.

Detection of Reactive Oxygen Species. FACS and fluorescent staining was performed for ROS detection in CAF by using DCFDA (Sigma-Aldrich). Cells were labeled with 10 μM H2-DCFDA for 30 min at 37 °C in the dark, and ROS production was monitored under fluorescence microscopy and quantified through flow cytometric analysis.

Catalase Activity Assay. Catalase activity was measured in CAF lysate by using a OxiSelect Catalase Activity Assay Kit (Cell Biolabs, San Diego) according to the manufacturer's protocol, and absorbance was taken at 520 nm in a 96-well plate. Ten millimolar of 3-amino-1,2,4-triazole (Santa Cruz Biotechnology) was used as a catalase inhibitor.

Statistical Analysis. Experiments were done a minimum of three times. Results are shown in terms of mean ± SD. Student's *t* test and one-way ANOVA were used for comparisons among groups, and repeated measured ANOVA was applied for determining the significance of two or more data series. Statistical tests using Origin software (OriginLab), are reported in the figure legends, along with the associated *P* values. Cell viability was examined using MTT assay as indicated by the manufacturer (Thermo Fisher); for the calculation of synergistic drug interactions, the Chou-Talalay method was performed (R Package).

Data Availability Statement. All data discussed in the paper are available in the main text and *SI Appendix*.

ACKNOWLEDGMENTS. We thank Dr. Manisha Tripathi for expert support in subcutaneous tumor grafting as well as advice from Drs. Krizia Rohena-Rivera and Bethany Smith. Manuscript editing was performed by Dr. Richard Suzuki. The work was supported in part by the National Cancer Institute grant CA098912 and Veterans Administration Merit Award I01BX001040 to N.A.B.

1. R. L. Siegel, K. D. Miller, A. Jemal, Cancer statistics, 2019. *CA Cancer J. Clin.* **69**, 7–34 (2019).
2. J. Qi *et al.*, The E3 ubiquitin ligase Siah2 contributes to castration-resistant prostate cancer by regulation of androgen receptor transcriptional activity. *Cancer Cell* **23**, 332–346 (2013).
3. V. R. Placencio *et al.*, Stromal transforming growth factor-beta signaling mediates prostatic response to androgen ablation by paracrine Wnt activity. *Cancer Res.* **68**, 4709–4718 (2008).
4. M. Kato *et al.*, Heterogeneous cancer-associated fibroblast population potentiates neuroendocrine differentiation and castrate resistance in a CD105-dependent manner. *Oncogene* **38**, 716–730 (2019).
5. N. A. Bhowmick *et al.*, TGF-beta signaling in fibroblasts modulates the oncogenic potential of adjacent epithelia. *Science* **303**, 848–851 (2004).
6. N. A. Bhowmick, Metastatic ability: Adapting to a tissue site unseen. *Cancer Cell* **22**, 563–564 (2012).
7. J. Banerjee *et al.*, A reciprocal role of prostate cancer on stromal DNA damage. *Oncogene* **33**, 4924–4931 (2014).
8. M. Gleave, J. T. Hsieh, C. A. Gao, A. C. von Eschenbach, L. W. Chung, Acceleration of human prostate cancer growth in vivo by factors produced by prostate and bone fibroblasts. *Cancer Res.* **51**, 3753–3761 (1991).
9. A. F. Olumi *et al.*, Carcinoma-associated fibroblasts direct tumor progression of initiated human prostatic epithelium. *Cancer Res.* **59**, 5002–5011 (1999).

10. S. W. Hayward *et al*., Malignant transformation in a nontumorigenic human prostatic epithelial cell line. *Cancer Res.* **61**, 8135–8142 (2001).
11. A. Calon *et al*., Dependency of colorectal cancer on a TGF-β-driven program in stromal cells for metastasis initiation. *Cancer Cell* **22**, 571–584 (2012).
12. C. L. Au Yeung *et al*., Exosomal transfer of stroma-derived miR21 confers paclitaxel resistance in ovarian cancer cells through targeting APAF1. *Nat. Commun.* **7**, 11150 (2016).
13. M. A. Kiskowski *et al*., Role for stromal heterogeneity in prostate tumorigenesis. *Cancer Res.* **71**, 3459–3470 (2011).
14. V. R. Minciacchi *et al*., MYC mediates large oncosome-induced fibroblast reprogramming in prostate cancer. *Cancer Res.* **77**, 2306–2317 (2017).
15. A. A. Donjacour, A. Rosales, S. J. Higgins, G. R. Cunha, Characterization of antibodies to androgen-dependent secretory proteins of the mouse dorsolateral prostate. *Endocrinology* **126**, 1343–1354 (1990).
16. A. A. Donjacour, G. R. Cunha, Assessment of prostatic protein secretion in tissue recombinants made of urogenital sinus mesenchyme and urothelium from normal or androgen-insensitive mice. *Endocrinology* **132**, 2342–2350 (1993).
17. M. E. Fiori *et al*., Cancer-associated fibroblasts as abettors of tumor progression at the crossroads of EMT and therapy resistance. *Mol. Cancer* **18**, 70 (2019).
18. R. Mishra *et al*., Stromal epigenetic alterations drive metabolic and neuroendocrine prostate cancer reprogramming. *J. Clin. Invest.* **128**, 4472–4484 (2018).
19. M. A. Jordan, L. Wilson, Microtubules as a target for anticancer drugs. *Nat. Rev. Cancer* **4**, 253–265 (2004).
20. I. F. Tannock *et al*.; TAX 327 Investigators, Docetaxel plus prednisone or mitoxantrone plus prednisone for advanced prostate cancer. *N. Engl. J. Med.* **351**, 1502–1512 (2004).
21. D. Rathkopf *et al*., Phase II trial of docetaxel with rapid androgen cycling for progressive noncastrate prostate cancer. *J. Clin. Oncol.* **26**, 2959–2965 (2008).
22. M. T. Schweizer *et al*., Adjuvant leuprolide with or without docetaxel in patients with high-risk prostate cancer after radical prostatectomy (TAX-3501): Important lessons for future trials. *Cancer* **119**, 3610–3618 (2013).
23. C. J. Sweeney *et al*., Chemohormonal therapy in metastatic hormone-sensitive prostate cancer. *N. Engl. J. Med.* **373**, 737–746 (2015).
24. N. D. James *et al*.; STAMPEDE investigators, Addition of docetaxel, zoledronic acid, or both to first-line long-term hormone therapy in prostate cancer (STAMPEDE): Survival results from an adaptive, multiarm, multistage, platform randomised controlled trial. *Lancet* **387**, 1163–1177 (2016).
25. U. E. Martinez-Outschoorn, S. Pavlides, F. Sotgia, M. P. Lisanti, Mitochondrial biogenesis drives tumor cell proliferation. *Am. J. Pathol.* **178**, 1949–1952 (2011).
26. J. A. Petros *et al*., mtDNA mutations increase tumorigenicity in prostate cancer. *Proc. Natl. Acad. Sci. U.S.A.* **102**, 719–724 (2005).
27. J. Ellinger, S. C. Müller, N. Wernert, A. von Ruecker, P. J. Bastian, Mitochondrial DNA in serum of patients with prostate cancer: A predictor of biochemical recurrence after prostatectomy. *BJU Int.* **102**, 628–632 (2008).
28. M. C. Caino *et al*., Syntaphilin controls a mitochondrial rheostat for proliferation-motility decisions in cancer. *J. Clin. Invest.* **127**, 3755–3769 (2017).
29. K. Grupp *et al*., High mitochondria content is associated with prostate cancer disease progression. *Mol. Cancer* **12**, 145 (2013).
30. A. Moore *et al*., A prospective study of mitochondrial DNA copy number and the risk of prostate cancer. *Cancer Causes Control* **28**, 529–538 (2017).
31. H. C. Lee *et al*., Mitochondrial genome instability and mtDNA depletion in human cancers. *Ann. N. Y. Acad. Sci.* **1042**, 109–122 (2005).
32. W. Zhou *et al*., Peripheral blood mitochondrial DNA copy number is associated with prostate cancer risk and tumor burden. *PLoS One* **9**, e109470 (2014).
33. S. Bhattacharyya *et al*., TLR4-dependent fibroblast activation drives persistent organ fibrosis in skin and lung. *JCI Insight* **3**, 98850 (2018).
34. C. Yao *et al*., Toll-like receptor family members in skin fibroblasts are functional and have a higher expression compared to skin keratinocytes. *Int. J. Mol. Med.* **35**, 1443–1450 (2015).
35. R. Cheng *et al*., Periodontal inflammation recruits distant metastatic breast cancer cells by increasing myeloid-derived suppressor cells. *Oncogene* **39**, 1543–1556 (2020).
36. D. A. Muruve *et al*., The inflammasome recognizes cytosolic microbial and host DNA and triggers an innate immune response. *Nature* **452**, 103–107 (2008).
37. M. Chiba, S. Kubota, K. Sato, S. Monzen, Exosomes released from pancreatic cancer cells enhance angiogenic activities via dynamin-dependent endocytosis in endothelial cells in vitro. *Sci. Rep.* **8**, 11972 (2018).
38. M. H. Lahoud *et al*., DEC-205 is a cell surface receptor for CpG oligonucleotides. *Proc. Natl. Acad. Sci. U.S.A.* **109**, 16270–16275 (2012).
39. E. Bonavita *et al*., PTX3 is an extrinsic oncosuppressor regulating complement-dependent inflammation in cancer. *Cell* **160**, 700–714 (2015).
40. P. F. Zipfel, C. Skerka, Complement regulators and inhibitory proteins. *Nat. Rev. Immunol.* **9**, 729–740 (2009).
41. L. G. Coulthard, T. M. Woodruff, Is the complement activation product C3a a proinflammatory molecule? Re-evaluating the evidence and the myth. *J. Immunol.* **194**, 3542–3548 (2015).
42. M. Shingu *et al*., Activation of complement in normal serum by hydrogen peroxide and hydrogen peroxide-related oxygen radicals produced by activated neutrophils. *Clin. Exp. Immunol.* **90**, 72–78 (1992).
43. M. S. Cho *et al*., Autocrine effects of tumor-derived complement. *Cell Rep.* **6**, 1085–1095 (2014).
44. S. C. Bischoff, A. L. de Weck, C. A. Dahinden, Interleukin 3 and granulocyte/macrophage-colony-stimulating factor render human basophils responsive to low concentrations of complement component C3a. *Proc. Natl. Acad. Sci. U.S.A.* **87**, 6813–6817 (1990).
45. G. Nilsson *et al*., C3a and C5a are chemotaxins for human mast cells and act through distinct receptors via a pertussis toxin-sensitive signal transduction pathway. *J. Immunol.* **157**, 1693–1698 (1996).
46. P. J. Daffern, P. H. Pfeifer, J. A. Ember, T. E. Hugli, C3a is a chemotaxin for human eosinophils but not for neutrophils. I. C3a stimulation of neutrophils is secondary to eosinophil activation. *J. Exp. Med.* **181**, 2119–2127 (1995).
47. M. L. Novak, E. M. Weinheimer-Haus, T. J. Koh, Macrophage activation and skeletal muscle healing following traumatic injury. *J. Pathol.* **232**, 344–355 (2014).
48. T. Werfel *et al*., Activated human T lymphocytes express a functional C3a receptor. *J. Immunol.* **165**, 6599–6605 (2000).
49. K. H. Lim, L. M. Staudt, Toll-like receptor signaling. *Cold Spring Harb. Perspect. Biol.* **5**, a011247 (2013).
50. M. Wang *et al*., Microbial hijacking of complement-toll-like receptor crosstalk. *Sci. Signal.* **3**, ra11 (2010).
51. R. W. Chiu *et al*., Quantitative analysis of circulating mitochondrial DNA in plasma. *Clin. Chem.* **49**, 719–726 (2003).
52. M. Yu, Circulating cell-free mitochondrial DNA as a novel cancer biomarker: Opportunities and challenges. *Mitochondrial DNA* **23**, 329–332 (2012).
53. D. Torralba *et al*., Priming of dendritic cells by DNA-containing extracellular vesicles from activated T cells through antigen-driven contacts. *Nat. Commun.* **9**, 2658 (2018).
54. Y. Wang *et al*., Autocrine complement inhibits IL10-dependent T-cell-mediated antitumor immunity to promote tumor progression. *Cancer Discov.* **6**, 1022–1035 (2016).
55. B. Ingelsson *et al*., Lymphocytes eject interferogenic mitochondrial DNA webs in response to CpG and non-CpG oligodeoxynucleotides of class C. *Proc. Natl. Acad. Sci. U.S.A.* **115**, E478–E487 (2018).
56. J. Mikuła-Pietrasik *et al*., Comprehensive review on how platinum- and taxane-based chemotherapy of ovarian cancer affects biology of normal cells. *Cell. Mol. Life Sci.* **76**, 681–697 (2019).
57. F. Leulier, B. Lemaitre, Toll-like receptors: Taking an evolutionary approach. *Nat. Rev. Genet.* **9**, 165–178 (2008).
58. S. Haldar *et al*., Inflammation and pyroptosis mediate muscle expansion in an interleukin-1β (IL-1β)-dependent manner. *J. Biol. Chem.* **290**, 6574–6583 (2015).
59. S. Haldar *et al*., Histone deacetylase inhibitors mediate DNA damage repair in ameliorating hemorrhagic cystitis. *Sci. Rep.* **6**, 39257 (2016).